

Effect of N-Methylation of Macrocyclic Amine Ligands on the Spin State of Iron(III): A Tale of Two Fluoro Complexes

John F. Berry, Eckhard Bill, Ricardo García-Serres, Frank Neese, Thomas Weyhermüller, and Karl Wieghardt*

Max-Planck-Institut für Bioanorganische Chemie, Stiftstrasse 34-36,
D-45470 Mülheim an der Ruhr, Germany

Received October 21, 2005

Syntheses and characterization of [(cyclamacetate)FeF]PF₆ (**1**) and the corresponding N-methylated complex [(trimethylcyclamacetate)FeF]PF₆ (**3**) are presented. Compound **1** is prepared in good yields from the analogous chloro complex, whereas **3** is prepared by hydrolysis of the oxo-bridged diiron compound (Me₃cyclam-acetate)-Fe–O–FeCl₃ (**2**) in the presence of PF₆ anions. Magnetic susceptibility and spectroscopic data including electron paramagnetic resonance and Mössbauer spectra indicate that **1** contains low-spin Fe^{III} ($S = 1/2$), while **3** is high spin ($S = 5/2$). Both octahedral fluoro complexes were investigated theoretically by density functional theory in order to determine why the spin states of the two molecules are different. Energies calculated using the B3LYP functional correctly predict **1** to have a low-spin $S = 1/2$ ground state and **3** to be high spin, regardless of whether a solvation model is included. The difference between **1** and **3** is most likely a combination of steric effects caused by the N-methyl groups, which compel the Fe–N bond distances to be longer in **3** than they ordinarily would be, and also electronic effects, which cause the N-methylated ligand to be a weaker σ donor than its nonmethylated counterpart.

Introduction

Iron is the most important transition metal found in biological systems and plays various roles in many important life processes.¹ The versatility of iron in biology stems from its versatility as a metal ion. For example, iron can exist in variable oxidation states, with iron(II) and iron(III) being the most prevalent in biological systems, though low-valent iron is known in systems such as hydrogenases² and important intermediates in oxygen-activating enzymes are known to involve iron(IV).³ Another feature of iron is the availability of several spin states within each oxidation state, each leading to different electronic structures and therefore different reactivities. In general, the spin state is governed

by the ligand field strength, but for complexes with more than one type of ligand, this is a complex effect whose subtleties are often difficult to define. For heme complexes, the influence of many different axial ligands has been extensively studied and an empirical “magnetochemical series” has been proposed.⁴ The advantage of the porphyrin studies is that the equatorial ligand can be assumed to have a fixed ligand field strength, and thus the effects of only the axial ligands can be probed. For iron complexes without porphyrin ligands such as models for nonheme iron enzymes, however, no such assumption can be made.

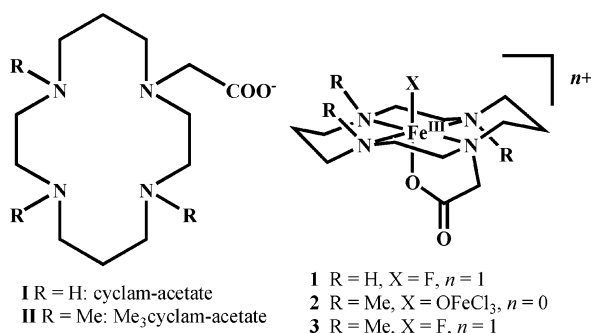
Recently, iron complexes of the cyclamacetate ligand (**I**; see Chart 1) have been of interest because the ligand supports an octahedral geometry and occupies the four equatorial coordination sites with amine nitrogen atoms and has a carboxylate arm that coordinates to a fifth site, leaving one site open for a sixth ligand.^{5,6} In our past work, we have found that this ligand stabilizes octahedral iron complexes

* To whom correspondence should be addressed. E-mail: wieghardt@mpi-muelheim.mpg.de.

(1) Lippard, S. J.; Berg, J. M. *Principles of Bioinorganic Chemistry*; University Science Books: Mill Valley, CA, 1994.
(2) Darensbourg, M. Y.; Lyon, E. J.; Smee, J. J. *Coord. Chem. Rev.* **2000**, *206*, 533.
(3) (a) Costas, M.; Mehn, M. P.; Jensen, M. P.; Que, L. *Chem. Rev.* **2004**, *104*, 939. (b) Merckx, M.; Kopp, D. A.; Sazinsky, M. H.; Blazyk, J. L.; Müller, J.; Lippard, S. J. *Angew. Chem., Int. Ed.* **2001**, *40*, 2782.
(c) Fujii, H. *Coord. Chem. Rev.* **2002**, *226*, 51. (d) Nakamoto, K. *Coord. Chem. Rev.* **2002**, *226*, 153. (e) Price, J. C.; Barr, E. W.; Tirupati, B.; Bollinger, J. M.; Krebs, C. *Biochemistry* **2003**, *42*, 7497.

(4) (a) Scheidt, W. R.; Reed, C. A. *Chem. Rev.* **1981**, *81*, 543. (b) Scheidt, W. R.; Osvath, S. R.; Lee, Y. J.; Reed, C. A.; Shaevitz, B.; Gupta, G. P. *Inorg. Chem.* **1989**, *28*, 1591. (c) Evans, D. R.; Reed, C. A. *J. Am. Chem. Soc.* **2000**, *122*, 4660.
(5) (a) Szulbinski, W. S.; Busch, D. H. *Inorg. Chim. Acta* **1995**, *234*, 143. (b) Szulbinski, W. S. *Pol. J. Chem.* **2000**, *74*, 1163.

Chart 1

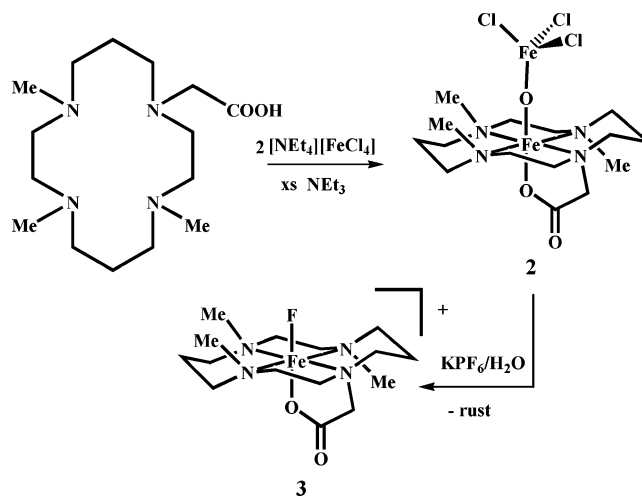


with various sixth ligands in a low-spin configuration in the oxidation states 2+, 3+, 4+, and 5+.^{6–8} Because of our interest in the highly oxidized iron(IV) and iron(V) species, methods to further stabilize the high-valent states were sought. Following the recent report of the crystal structure of an iron(IV) oxo containing species using the *N*-methylated tetramethylcyclam ligand by the group of Que et al.,⁹ we decided to modify the ligand **I** by the addition of *N*-methyl groups to see if the added methyl groups indeed stabilize the higher oxidation states. Thus, the ligand trimethylcyclam-acetate (**II**) was synthesized, and its iron complexes have been shown to exhibit two remarkable properties: whereas all known compounds utilizing **I** are low-spin, ferrous and ferric complexes of **II** are high-spin, and also compounds of **II** can be reversibly oxidized to iron(IV), whereas the nonmethylated analogues cannot.¹⁰

The former observation is related to work done by the Meyerstein group¹¹ mainly on nickel and chromium complexes of macrocyclic ligands with or without *N*-alkyl groups. Meyerstein's result that *N*-alkylated ligands are in general weaker-field ligands than their nonalkylated analogues is reported to be the result of four combined and competing effects:¹¹ (1) stabilization of nonalkylated complexes via solvation; (2) stabilization of nonalkylated complexes via M–N–H···S hydrogen bonds (S = solvent); (3) steric hindrance in alkylated complexes; (4) electron-donating effects of the alkyl substituents causing alkylated ligands to be better σ donors.

Reported in this paper is a combined experimental/theoretical study of similar effects in iron compounds that involves synthesis and characterization of new analogous complexes (see Chart 1) of the ligands **I** and **II**, namely, [(cyclamacetate)FeF]PF₆ (**1**) and [(trimethylcyclamacetate)–FeF]PF₆ (**3**), and calculation of their properties using density functional theory (DFT).

Scheme 1



Results and Discussion

Synthesis. The ligand **I** was synthesized according to the procedure reported by Studer and Kaden,¹² and **II** is easily synthesized from **I**·4HCl in high yields by the Eschweiler–Clarke reaction using acidic formaldehyde. The salt **II**·4HCl can be crystallized from HCl/EtOH mixtures.

The fluoro complex **1** was synthesized in good yield from its chloro analogue, [(cyclamacetate)FeCl]PF₆, by reaction with AgPF₆ in refluxing methanol. After filtration of the insoluble AgCl, water was added to the filtrate and pale-pink hexagonal crystals of **1**·MeOH grew from the solution upon standing for 48 h. The fluoro anions originate from slow hydrolysis of PF₆[–] in an aqueous solution, as has been reported in a number of instances.¹³

The reaction of **II**·4HCl with FeCl₃ in the presence of 5 equiv of base (either NEt₃ or LiOH) afforded only rust. The reaction was, therefore, carried out in more controlled conditions using [NEt₄][FeCl₄] as a neutral source of iron (because the addition of FeCl₃ typically releases HCl in solution) and initially 4 equiv of NEt₃. This results immediately in complexation of the iron, yielding a brown solution, which slowly becomes red upon heating. The addition of a further excess amount of base allows the reaction to go to completion with minimal rusty side products. Surprisingly, this reaction does not yield the anticipated chloro complex but instead yields a deep-red oxo-bridged diiron complex, (trimethylcyclamacetate)Fe–O–FeCl₃ (**2**; see Scheme 1). Many previous examples of compounds containing an Fe–O–FeCl₃ moiety have been described.¹⁴ It was found here that hydrolysis of the –O–FeCl₃ group can be achieved in water by the addition of KPF₆, yielding a ruddy-brown iron oxide precipitate and a

(6) Grapperhaus, C. A.; Mienert, B.; Bill, E.; Weyhermüller, T.; Wieghardt, K. *Inorg. Chem.* **2000**, *39*, 5306.

(7) García-Serres, R.; Grapperhaus, C. A.; Bothe, E.; Bill, E.; Weyhermüller, T.; Neese, F.; Wieghardt, K. *J. Am. Chem. Soc.* **2004**, *126*, 5138.

(8) Aliaga-Alcalde, M.; George, S. D.; Mienert, B.; Bill, E.; Wieghardt, K.; Neese, F. *Angew. Chem., Int. Ed.* **2005**, *44*, 2908.

(9) Rohde, J. U.; In, J. H.; Lim, M. H.; Brennessel, W. W.; Bukowski, M. R.; Stubna, A.; Münck, E.; Nam, W.; Que, L. *Science* **2003**, *299*, 1037.

(10) Berry, J. F.; Bill, E.; Bothe, E.; Weyhermüller, T.; Wieghardt, K. *J. Am. Chem. Soc.* **2005**, *127*, 11550.

(11) Meyerstein, D. *Coord. Chem. Rev.* **1999**, *186*, 141.

(12) Studer, M.; Kaden, T. A. *Helv. Chim. Acta* **1986**, *69*, 2081.

(13) (a) Gebala, A. E.; Jones, M. M. *J. Inorg. Nucl. Chem.* **1969**, *31*, 771. (b) Matsumoto, K.; Sano, Y.; Kawano, M.; Uemura, H.; Matsunami, J.; Sato, T. *Bull. Chem. Soc. Jpn.* **1997**, *70*, 1239. (c) Ghiladi, M.; Jensen, K. B.; Jiang, J. Z.; McKenzie, C. J.; Morup, S.; Sotofte, I.; Ulstrup, J. *J. Chem. Soc., Dalton Trans.* **1999**, 2675. (d) Ghiladi, M.; McKenzie, C. J.; Meier, A.; Powell, A. K.; Ulstrup, J.; Wocadlo, S. *J. Chem. Soc., Dalton Trans.* **1997**, 4011. (e) Zang, Y.; Jang, H. G.; Chiou, Y. M.; Hendrich, M. P.; Que, L. *Inorg. Chim. Acta* **1993**, *213*, 41.

Table 1. Selected Bond Distances (Å) and Angles (deg) in **1–3**

	1	2^a	3
Fe–L _{ax}	1.841(2)	1.802(2)	1.848(2)
Fe–N _{av}	2.001(2)	2.174(4)	2.148(2)
Fe–O	1.886(2)	2.047(2)	1.979(2)
O–Fe–L _{ax}	178.0(1)	173.7(1)	175.5(1)
Fe2–O		1.763(2)	
Fe2–Cl _{av}		2.236(1)	
Fe1–O–Fe2		173.2(1)	

^a Values for only the major orientation are given.

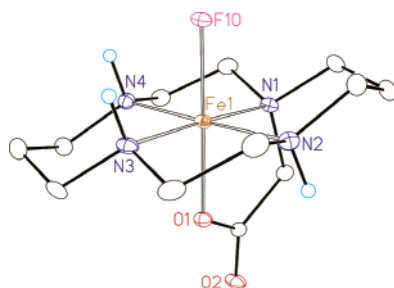


Figure 1. Thermal ellipsoid plot of the cation of **1** with ellipsoids drawn at the 30% probability level and all hydrogen atoms removed except for the amine hydrogen atoms, which are shown in light blue.

clear-yellow solution. Slow evaporation of the water solution (accompanied by hydrolysis of the PF₆[−] anions) yields small platelike crystals of **3**, [(trimethylcyclamacetate)FeF]PF₆.

Crystal Structures. In all three structures reported here, the modified cyclam ligands bind the ferric ions in the thermodynamically most favorable trans conformation.¹⁵ The pendant acetate arms occupy one axial position while the other axial position is occupied by either a fluoride ion (in the case of **1** and **3**) or an OFeCl₃ group in the case of **2**. Selected bond distances and angles for **1–3** are listed in Table 1.

The structure of **1** (Figure 1) is similar to that of the other structurally characterized iron(III) complex of the ligand **I**, namely, [(cyclamacetate)FeN₃]PF₆.⁶ Both complexes have an axially compressed octahedral geometry with Fe–N distances of 2.00 Å and an Fe–O bond distance of 1.89 Å to the pendant arm carboxylate. The Fe–F distance in **1** [1.841(2) Å] is considerably shorter than the corresponding Fe–N₃ distance [1.931(2) Å] in the azido complex, indicating a greater affinity of the iron(III) center for the fluoride ion,

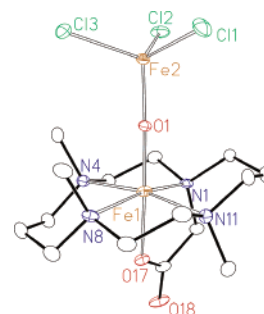
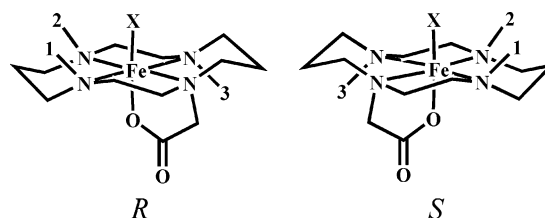


Figure 2. Thermal ellipsoid plot of the major orientation of **2** from its crystal structure. The ellipsoids are drawn at the 30% probability level, and hydrogen atoms are removed.

Chart 2

which is a harder base than azide. The metal–ligand distances in **1** indicate a low-spin configuration for the iron. The structure also includes a molecule of methanol in the asymmetric unit, which has hydrogen-bonding interactions with the uncoordinated oxygen atom of the acetate arm and with one of the amino groups of the ligand.

The oxo-bridged compound **2** crystallizes in the chiral space group *P*2₁2₁2₁. Though the crystal is not a racemic twin [the Flack parameter refined to a value of 0.012(14)], the entire trimethylcyclamacetate ligand is disordered in the structure such that both enantiomers of the compound are present, with the *S* enantiomer having a larger occupancy (~60%). Here the *R* and *S* enantiomers are defined based on the position of the methyl groups, as shown in Chart 2.

Viewing the molecule down the X–Fe–O axis, the methyl groups are counted contiguously starting from the two that are next to each other and ending with the one that is on the other side of the macrocyclic plane. If the counting occurs in a clockwise direction, this is the *R* isomer, and if it is done in a counterclockwise direction, this is the *S* isomer. The *S* enantiomer of compound **2** is shown in Figure 2.

The bridging oxo ligand forms short bonds to both iron atoms in the structure [1.802(2) Å to Fe1 and 1.763(2) to Fe2], and the Fe–O–Fe angle of 173.2(1)^o is nearly linear such that π bonding through the Fe–O–Fe unit is possible. The coordinated acetate oxygen atom, which is trans to the μ -oxo ligand, has a longer distance of 2.047(2) Å to the iron atom because of the strong trans influence of the oxo ligand. Interestingly, the average Fe–N distance to the ligand **II** of 2.174(4) Å is 0.17 Å longer than the Fe–N distance observed in the compounds of ligand **I**, which suggests that the octahedrally coordinated iron atom in **2** is high-spin rather than low-spin.

Compound **3** (Figure 3) also has rather long Fe–N bond distances of 2.148(2) Å also indicative of a high-spin ferric ion, though the Fe–F distance of 1.848(2) Å is not

- (14) (a) Gómez-Romero, P.; DeFotis, G. C.; Jameson, G. B. *J. Am. Chem. Soc.* **1986**, *108*, 851. (b) Gómez-Romero, P.; Witten, E. H.; Reiff, W. M.; Jameson, G. B. *Inorg. Chem.* **1990**, *29*, 5211. (c) Borzel, H.; Comba, P.; Hagen, K. S.; Lampeka, Y. D.; Lienke, A.; Linti, G.; Merz, M.; Pritzkow, H.; Tsybmal, L. V. *Inorg. Chim. Acta* **2002**, *337*, 407. (d) Moll, N.; Banse, F.; Miki, K.; Nierlich, M.; Girerd, J. J. *Eur. J. Inorg. Chem.* **2002**, 1941. (e) Balland, V.; Banse, F.; Anxolabéhère-Mallart, E.; Ghiladi, M.; Mattioli, T. A.; Philouze, C.; Blondin, G.; Girerd, J. J. *Inorg. Chem.* **2003**, *42*, 2470. (f) Liu, X. M.; Kilner, C. A.; Halcrow, M. A. *Acta Crystallogr., Sect. C: Cryst. Struct. Commun.* **2002**, *58*, m290. (g) Gómez-Romero, P.; Witten, E. H.; Reiff, W. M.; Backes, G.; Sandersloehr, J.; Jameson, G. B. *J. Am. Chem. Soc.* **1989**, *111*, 9039. (h) Wang, J. P.; Mashuta, M. S.; Sun, Z. M.; Richardson, J. F.; Hendrickson, D. N.; Buchanan, R. M. *Inorg. Chem.* **1996**, *35*, 6642. (i) Ondrejčková, I.; Lis, T.; Mroziński, J.; Vaněová, V.; Melník, M. *Polyhedron* **1998**, *17*, 3181. (j) Ondrejčková, I.; Lis, T.; Mroziński, J.; Vaněová, V.; Melník, M. *Inorg. Chim. Acta* **1998**, *277*, 127. (k) James, M.; Kawaguchi, H.; Tatsumi, K. *Polyhedron* **1997**, *16*, 4279.
- (15) Adam, K. R.; Atkinson, I. M.; Lindoy, L. F. *Inorg. Chem.* **1997**, *36*, 480.

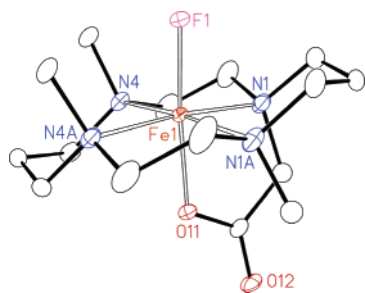


Figure 3. Structure of the cation of **3** with thermal ellipsoids drawn at the 30% probability level and hydrogen atoms removed.

significantly different from the Fe–F distance of 1.842(1) Å in **1**. The Fe–O distance of 1.979(2) Å, however, is nearly 0.1 Å longer than that observed in **1**, also indicating that **3** is high-spin. It should be noted that **3** crystallizes on a site of mirror symmetry (space group *Pnma*), with the mirror plane passing through the O–Fe–F unit and the central carbon atoms of each of the propylene units of the macrocyclic ligand. Thus, the asymmetric unit contains a half-molecule, and there are only two unique Fe–N bond distances. The acetate group is disordered, yielding a superposition of the *R* and *S* enantiomers.

Magnetic Susceptibility and Electron Paramagnetic Resonance (EPR) Measurements. The magnetic susceptibility of **1** was measured in the range of 2–380 K, and a plot of χT vs *T* is shown in Figure 4. The low-temperature value of 0.5 emu K mol⁻¹ is consistent with the low-spin assignment [$S = 1/2$; $\chi T(\text{spin only}) = 0.375$ emu K mol⁻¹], but it should be noted that above 250 K the value of χT rises as the temperature is increased, suggesting a spin-crossover phenomenon. It was found that, above 350 K, the sample decomposes, but the behavior from 250 to 350 K was reproduced in separate samples. Similar magnetic susceptibility plots indicative of spin crossover were seen for the other iron(III) complexes of cyclamacetate, but we had not analyzed this phenomenon in detail in our previous work.⁶ The susceptibility data could be simulated using a spin-crossover model¹⁶ (assuming an ideal solution of spin carriers), with the low-spin species having $S = 1/2$ and the high-spin species having $S = 5/2$, using eq 1.

$$\chi T = (1-p) \left\{ \frac{g_{\text{HS}}^2 C_{\text{HS}} - \frac{g_{\text{LS}}^2 C_{\text{LS}} T}{4(T-\theta)}}{1 + \exp\left[\frac{\Delta H}{R} \left(\frac{1}{T} - \frac{1}{T_C}\right)\right]} + \frac{g_{\text{LS}}^2 C_{\text{LS}} T}{4(T-\theta)} \right\} + p\chi_p T \quad (1)$$

In this equation, g_{HS} and g_{LS} are the isotropic Landé factors for the high- and low-spin states, respectively, and C_{HS} and C_{LS} are their respective Curie constants (4.375 and 0.375 emu K mol⁻¹, respectively), θ is the Weiss constant (fixed at a value of -1.0 K), which accounts for weak intramolecular interactions and field saturation effects, ΔH is the enthalpy change of the spin-crossover process, R is the gas

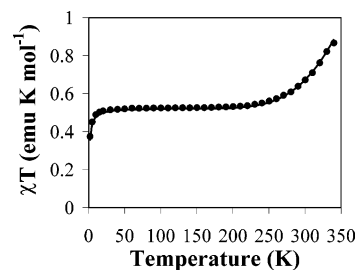


Figure 4. Temperature dependence of χT (corrected for diamagnetism and TIP) for compound **1** from 2 to 350 K. At 350 K, the sample contains 90% of low-spin Fe^{III} and 10% of high-spin Fe^{III}. The solid line is a simulation of a high-spin/low-spin transition (see text), which includes a 1% paramagnetic impurity with $S = 5/2$.

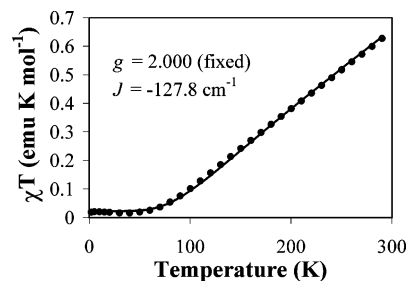


Figure 5. Plot of χT vs *T* for **2**. The solid line represents the theoretical fit of the data (corrected for diamagnetism and TIP) as discussed in the text. Values of *g* and *J* are given in the inset, and the model also includes a 0.5% paramagnetic impurity with $S = 5/2$.

constant, T_C is the critical temperature (i.e., the temperature at which equal amounts of high- and low-spin species are present), *p* is the percentage of a paramagnetic impurity (1% with $S = 5/2$), and $\chi_p T$ is the temperature-independent value of 4.375 emu K mol⁻¹ for the paramagnetic impurity. Because there is only a small population of the high-spin state at the highest temperatures measured (~10%), g_{HS} was fixed at 2.00 (g_{LS} was fixed at 2.25, the average of the three *g* values observed in the EPR spectrum, vide infra). The values of ΔH and T_C are highly correlated because of the incompleteness of the curve and were set to 20 kJ mol⁻¹ and 500 K, respectively. Despite the uncertainty of ΔH and T_C , it is clear that the magnetic susceptibility of **1** can be simulated by a model in which the compound undergoes spin crossover.

Figure 5 shows the plot of χT vs *T* for compound **2**. Between 2 and 50 K, a value near zero is observed, indicating a diamagnetic ground state, though the value of χT increases steadily with temperature, reaching a value of 0.6 emu K mol⁻¹ at 300 K. The behavior is consistent with strong antiferromagnetic coupling of two $S = 5/2$ ferric ions, which could be modeled with the spin Hamiltonian $H = -2JS_1S_2$. A *J* value of -128 cm⁻¹ is found in the fitting, which compares well with the values found in other oxo-bridged diiron(III) complexes.¹⁴

The magnetic data for **3** follow the Curie–Weiss law for $S = 5/2$, indicating the high-spin state of the compound. Both **1** and **3** are EPR-active and show broad spectra in a frozen nitrile solution, and these are shown in Figure 6. The spectrum of **1** shows a rhombic derivative pattern with widely split *g* values in the range from 1.6 to 3.0. The major part of the spectrum could be simulated with the assumption of *S*

(16) (a) Kahn, O. *Molecular Magnetism*; Wiley-VCH: New York, 1993.
(b) Berry, J. F.; Cotton, F. A.; Lu, T. B.; Murillo, C. A. *Inorg. Chem.* **2003**, *42*, 4425.

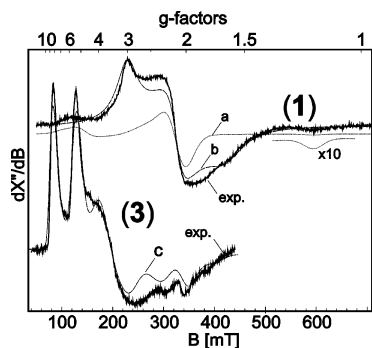


Figure 6. X-band EPR spectra of complexes **1** and **3** in an acetonitrile solution. The bold lines represent experimental data measured at $T = 10$ K, microwave frequency = 9.633 55 and 9.635 35 GHz, power 25 and 100 μ W, modulation 1 and 8 mT, respectively. The dashed lines labeled b and c are spin-Hamiltonian simulations for $S = 1/2$ and $5/2$, respectively; the line labeled a is an alternative simulation for a hypothetical triplet species with $S = 1$, which may arise from weak intermolecular spin-coupling and dipolar interaction (the relative amount of part b is ca. 25%, $D = 0.12$ cm^{-1} , $E/D = 0.3$, and $g = 3.1, 2.11, \text{ and } 1.63$).

$= 1/2$ and the rhombic factors $g = 3.00, 2.109, \text{ and } 1.63$ and Lorentzian lines of width $W = 120, 40, \text{ and } 80$ mT (see trace b in Figure 6, top). The anisotropy of the g values is expected for a low-spin ferric compound. The spectrum of **1** shows in addition to the main component two weak satellite lines at about $g = 1.2$ and 6, which are reminiscent of a spin-coupling pattern. In fact, a provisional simulation with a hypothetical spin-triplet species explains this feature (trace a in Figure 6, top, having a relative amount of about 25% integrated intensity). Thus, we suggest that some of the molecules in the frozen solution arrange as spin pairs that show weak intermolecular spin coupling, probably via the fluoride or acetate ligands. Compound **3** in a frozen butyronitrile solution shows g values well above 2. Two distinct peaks are observed in the derivative spectrum at about $g_{\text{eff}} = 5.3$ and 8.5. These resonances can be roughly assigned to the effective g_y and g_z values of the $|S = 5/2, m_S = \pm 1/2\rangle$ and $|S = 5/2, m_S = \pm 3/2\rangle$ Kramers doublet of a high-spin iron(III) complex with zero-field splitting larger than the Zeeman effect (see the rhombogram in Figure S1 of the Supporting Information). The derivative peaks at the other effective g values of the corresponding Kramers doublets are excessively broadened by g strain (see the “unbroadened” spectrum given as Figure S2 in the Supporting Information). The unusual shape of the spectrum can, nevertheless, be simulated by using the corresponding spin Hamiltonian for $S = 5/2$ with rhombic zero-field-splitting terms, $D = 0.4$ cm^{-1} and $E/D = 0.13$, and a Gaussian distribution of the rhombicity parameter E/D with a distribution of $\sigma(E/D) = 0.047$ (Figure 6, bottom). The value of the axial zero-field-splitting parameter D , which parametrizes the main splitting of the Kramers doublets, could be nicely determined from the relative intensities of the resolved peaks at $g_{\text{eff}} = 5.3$ and 8.5 because these belong to different doublets.

^{57}Fe Mössbauer Spectra. The zero-field Mössbauer spectra of **1** and **3** taken on solid samples are shown in Figure 7 along with the spectrum of **2** and an applied field spectrum of **3**. For **1**, the isomer shift (δ) of 0.25 mm s^{-1} measured at 80 K and a quadrupole splitting (ΔE_Q) of 2.67 mm s^{-1} are

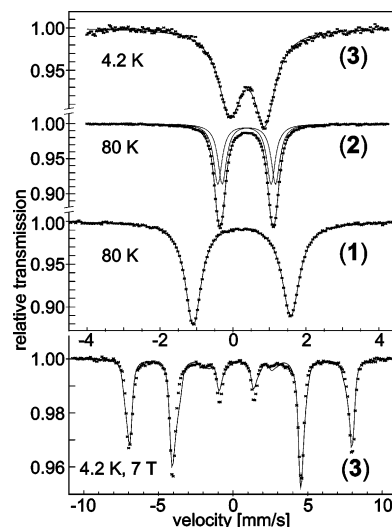


Figure 7. (Top) Zero-field Mössbauer spectra of compounds **1–3**. (Bottom) Magnetic Mössbauer spectrum of **3** at 4.2 K with a 7-T field applied perpendicularly to the γ -ray (bottom panel). The solid lines in the top panel are Lorentzian fits, whereas in the bottom spectrum, the solid line is the result of a spin-Hamiltonian simulation.

Table 2. Mössbauer Parameters for **1–3** and Other Complexes of the Two Ligands Used

	T, K	$\delta, \text{mm s}^{-1}$	$\Delta E_Q, \text{mm s}^{-1}$	$\Gamma, \text{mm s}^{-1}$	ref
[(cyclamacetate)FeCl]PF ₆	80	0.28	2.66	0.42	6
[(cyclamacetate)FeN ₃]PF ₆	80	0.27	2.53	0.64	6
[(cyclamacetate)FeOTf]PF ₆	80	0.26	2.82	0.95	6
1	80	0.25	2.67	0.55	this work
2^a (octahedral)	80	0.44	1.46	0.28	this work
2^a (tetrahedral)	80	0.32	1.46	0.29	this work
3	4.2	0.39	0.95	0.73	this work
[(trimethylcyclamacetate)-FeN ₃]PF ₆	200	0.35	0.84	0.47 ^b	10
	80	0.33	2.21	0.71	10

^a A second possible deconvolution with both species having the same isomer shift is possible and gives the following parameters: $\delta = 0.38$, $\Delta E_Q = 1.58$, $\Gamma = 0.27$; $\delta = 0.38$, $\Delta E_Q = 1.34$, $\Gamma = 0.30$. ^b $\Gamma(\text{R/L}) = 1.42$, $I(\text{R/L}) = 0.986$.

both in the expected range for low-spin iron(III) complexes and are quite similar to the values reported for the other known iron(III) complexes of the cyclamacetate ligand (see Table 2). The Mössbauer spectrum of the high-spin compound **3** at 80 K shows only very broad features, which have not been interpreted. The spectrum measured at 4 K is more useful and shows an isomer shift (0.39 mm s^{-1}) indicative of iron(III), and the quadrupole splitting of 0.95 mm s^{-1} is in the range expected for a typical octahedral high-spin iron(III) compound (which in a basic ligand-field picture has a quadrupole splitting close to 0 mm s^{-1} because of the vanishing orbital contribution of the 6S state ion). A Mössbauer spectrum of **3** in a frozen acetonitrile solution (1 mM, 40% enriched with ^{57}Fe) was measured in an applied magnetic field of 7 T (with the field perpendicular to the γ source) at 4 K to determine more accurately the Mössbauer and spin-Hamiltonian parameters. The spectrum was fitted using the same values of D and E/D as those found from the EPR spectrum (vide supra) and with hyperfine coupling tensor components $A_{xx} = A_{yy} = -21.3$ T (−29.4 MHz) and $A_{zz} = -21.0$ T (−29.0 MHz). The nature of the quadrupole-

splitting tensor is also determined from the applied field spectrum: the sign of ΔE_Q is negative ($\Delta E_Q = -0.92 \text{ mm s}^{-1}$), and the asymmetry parameter η is 0.4. Mössbauer spectra of **1** were measured at elevated temperatures to see if a signal due to the high-spin form of the molecule could be observed, but no second signal was found, presumably because of the low population of the high-spin state (<10% according to the susceptibility measurements).¹⁷

The Mössbauer spectrum of **2** is deceptively simple and consists of a single doublet. Although the line shape can be simulated by a single Lorentzian-shaped doublet, a more sensible simulation results in two overlapping doublets (one from each of the iron atoms in **2**), which have very similar isomer-shift and quadrupole-splitting parameters (see Figure 7). Two different deconvolutions of the spectrum are possible: one in which the two iron centers have the same isomer shift and another in which they have the same quadrupole splitting. The most reasonable model is the one in which both iron ions have the same quadrupole-splitting parameter (1.46 mm s^{-1}), which leads to isomer shifts of 0.44 and 0.32 mm s^{-1} for the two different iron centers. Furthermore, we can suggest that the species with an isomer shift of 0.44 mm s^{-1} is the iron complexed by the trimethylcyclamacetate ligand because the isomer shift is near those for other complexes of trimethylcyclamacetate (see Table 2).¹⁰ Thus, the species with an isomer shift of 0.32 mm s^{-1} is likely the tetrahedral O–FeCl₃ unit, and this value is nearly the same as that found in the Cl₃Fe–O–FeCl₃ dianion (0.33 mm s^{-1}).¹⁸ The other possible deconvolution of this spectrum yields isomer-shift values of 0.38 mm s^{-1} for both iron atoms and quadrupole-splitting values of 1.58 and 1.34 mm s^{-1} .

DFT Calculations. The fact that **1** is low-spin and **3** is high-spin despite a fairly minor change to the equatorial ligand represents an attractive test for the predictive power of DFT because of the availability of a considerable body of experimental data (vide supra). The question at hand is, can DFT predict the correct spin states for **1** and **3**? Previous investigations have indicated that spin-state energetics are particularly challenging for DFT methods, which tend to be biased in favor of low-spin states.¹⁹ While the use of some reparametrized functionals has been suggested,¹⁹ we prefer to base our studies on the established methods unless it becomes clear that the refitted functionals represent systematic improvements. Through this investigation, we can gain some insight into the effects that cause **1** and **3** to have different spin states, and we can make some comments about which of Meyerstein's four arguments listed above in the Introduction section are the most important for our iron complexes.

With this in mind, the cationic units from **1** and **3** (i.e., [(cyclamacetate)FeF]⁺ and [(trimethylcyclamacetate)FeF]⁺) were used for DFT calculations using the BP86 functional for geometry optimization and frequency calculations and the B3LYP functional for calculation of energies and other

Table 3. Experimental and Calculated Properties of [(Cyclamacetate)FeF]⁺

	experiment ($S = 1/2$)	$S = 1/2$		$S = 5/2$	
		double- ζ	triple- ζ	double- ζ	triple- ζ
Fe–F, Å	1.841(2)	1.842	1.859	1.864	1.880
Fe–N _{av} , Å	2.001(2)	2.032	2.029	2.181	2.174
Fe–O, Å	1.886(2)	1.877	1.877	1.961	1.959
O–Fe–F, deg	177.96(8)	179.1	179.3	170.5	171.3
relative E , eV			0	+28.99 kJ mol ⁻¹	
relative E including solvation, eV			0	+27.10 kJ mol ⁻¹	
$\nu(\text{C=O})$, cm ⁻¹	1661	1723		1709	
g	3.0, 2.1, 1.6	2.2, 2.1, 2.0		2.01	
D , cm ⁻¹ , E/D				1.266, 0.042	
δ , mm s ⁻¹	0.25	0.29		0.40	
ΔE_Q , mm s ⁻¹ , η	(–)2.67	–2.33, 0.14		–1.04, 0.41	

properties. Solvation effects were estimated using the COSMO model²⁰ because Clark et al. have attributed the effects of N-alkylation of macrocyclic ligands in nickel and chromium complexes mainly to a loss of solvation energy in the alkylated compounds.²¹

Geometries of the [(cyclamacetate)FeF]⁺ cation were optimized for the low- and high-spin forms with two different basis sets (double and triple ζ), and these results are compared to each other and to the experimental values in Table 3. From these data, it is easily concluded that changing the basis set from double- to triple- ζ quality does not significantly change any of the calculated bond distances (with the maximum difference between basis sets being $\sim 0.017 \text{ Å}$ for the Fe–F bond). Nevertheless, the triple- ζ geometries will be used for comparisons to the experimental values, and all other property calculations in Table 3 have been made on the triple- ζ -optimized geometries. It is interesting to point out the predicted changes in bond distances from the low-spin state to the high-spin state as calculated for this cation. From the $S = 1/2$ state to the $S = 5/2$ state, all of the Fe–ligand distances become longer, with the most dramatic changes being the lengthening of the Fe–N distances by 0.15 Å and the lengthening of the Fe–O distance by about 0.08 Å . These are the expected changes for population of the e_g orbitals, which are antibonding with respect to the ligands. Oddly, the Fe–F distance lengthens only by 0.02 Å in the high-spin state, but this change as well as the others is very similar to the observed differences in bond distances between the actual compounds **1** and **3**, which were investigated by X-ray crystallography. The calculated geometry of the low-spin cation [(cyclamacetate)FeF]⁺ agrees well with the observed geometry in the crystal structure of **1**. The largest deviation between the two structures is that the calculated average Fe–N bond distances are 0.028 Å longer than the observed distances, but this is not a major discrepancy.

(17) The variable-temperature Mössbauer spectra are given in the Supporting Information.

(18) Drew, M. G. B.; McKee, V.; Nelson, S. M. *J. Chem. Soc., Dalton Trans.* **1978**, 80.

(19) (a) Fouqueau, A.; Casida, M. E.; Daku, L. M. L.; Hauser, A.; Neese, F. *J. Chem. Phys.* **2005**, *122*, 044110. (b) Fouqueau, A.; Mer, S.; Casida, M. E.; Daku, L. M. L.; Hauser, A.; Mineva, T.; Neese, F. *J. Chem. Phys.* **2004**, *120*, 9473. (c) Ganzenmuller, G.; Berkaine, N.; Fouqueau, A.; Casida, M. E.; Reiher, M. *J. Chem. Phys.* **2005**, *122*, 234321.

(20) Klamt, A.; Schuurmann, G. *J. Chem. Soc., Perkin Trans. 2* **1993**, 799.

(21) Clark, T.; Hennemann, M.; van Eldik, R.; Meyerstein, D. *Inorg. Chem.* **2002**, *41*, 2927.

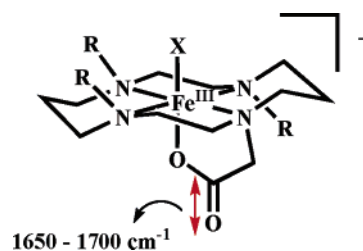
Table 4. Experimental and Calculated Properties of [(Trimethylcyclamacetate)FeF]⁺

	experiment (<i>S</i> = 5/2)	<i>S</i> = 1/2		<i>S</i> = 5/2	
		double- ζ	triple- ζ	double- ζ	triple- ζ
Fe–F, Å	1.848(2)	1.835	1.844	1.857	1.871
Fe–N _{av} , Å	2.148(2)	2.098	2.090	2.232	2.221
Fe–O, Å	1.979(2)	1.886	1.883	1.953	1.959
O–Fe–F, deg	175.5(1)	175.8	176.3	168.2	168.6
relative <i>E</i> , eV		+11.03 kJ/mol		0	
relative <i>E</i> including solvation, eV		+11.17 kJ/mol		0	
$\nu(\text{C=O})$, cm ⁻¹	1682	1714		1706	
<i>g</i> _{iso}	2.00	2.114		2.010	
<i>D</i> , cm ⁻¹ , <i>E/D</i>	0.4, 0.12			+0.898, 0.037	
δ , mm s ⁻¹	0.39	0.35		0.43	
ΔE_Q , mm s ⁻¹ , η	-0.95, 0.4	-2.35, 0.36		-1.22, 0.29	
<i>A</i> , MHz	-29.4, -29.4, -29.0			-31.3, -31.9, -32.0	

For the methylated [(trimethylcyclamacetate)FeF]⁺ cation, geometries of the (unobserved) *S* = 1/2 and (observed) *S* = 5/2 states were also optimized at the double- and triple- ζ levels (see Table 4). As with the nonmethylated species, the bond distances are not highly basis set dependent, and the major differences between the low- and high-spin structures are the longer Fe–N and Fe–O bond distances in the latter, as seen in the crystal structures of **1** and **3**. In a comparison of the calculated high-spin structure of [(trimethylcyclamacetate)FeF]⁺ to the structure observed in **3**, the Fe–F and Fe–O bond distances [1.848(2) and 1.979(2) Å, respectively] are well reproduced by the calculation (1.871 and 1.959 Å for the Fe–F and Fe–O distances, respectively), although it should be noted that the calculated average Fe–N distance of 2.221 Å is about 0.07 Å too long compared to the experimental distance [2.148(2) Å]. On the basis of our experience with the DFT methods used for closely related systems,^{7,22} this appears to be a systematic overestimation.

Not only do the geometries of **1** and **3** agree well with the calculated optimized geometries for low- and high-spin molecules, respectively, but the properties of **1** and **3**, which have been measured and discussed above, can also be reproduced through DFT calculations. In particular, vibrational, spin-Hamiltonian, and Mössbauer parameters have been calculated for the cations [(cyclamacetate)FeF]⁺ and [(trimethylcyclamacetate)FeF]⁺ in both the low- and high-spin configurations, and these data are all collected in Tables 3 and 4 along with the pertinent experimental data.

In principle, it should be possible to tell the low- and high-spin molecules apart from their vibrational spectra. The most prominent peaks in the IR spectra of **1** and **3** are those between 1650 and 1700 cm⁻¹, which we have assigned previously^{6,10} as bands due to the stretch of the C=O group of the molecule (see Chart 3). The C=O stretches are very characteristic for each complex because they are well isolated in the spectrum (and it is therefore unlikely that any other mode will influence the energy of this stretch through mixing) and are very intense. Because the experimental and calculated C=O double-bond distances (~1.230 and ~1.215 Å respectively) for the low- and high-spin species are not

Chart 3

significantly different from each other, a large difference in their C=O stretching frequencies is not to be expected, but because the Fe–O bond distance does change significantly on going from low spin to high spin, this is expected to change the nature of the π bonding in the C=O unit and may thus give rise to a measurable difference in the C=O stretching frequencies. Indeed, the experimental C=O stretching frequencies for **1** and **3** are 1661 and 1682 cm⁻¹, respectively, and the value for the high-spin compound is larger by 21 cm⁻¹. DFT does not quantitatively reproduce these results (all of the calculated C=O frequencies are above 1700 cm⁻¹), nor does it reproduce the qualitative trend that the low-spin species have lower C=O frequencies than their high-spin analogues. Thus, this effect is apparently too subtle for DFT to reproduce, at least with the level of theory employed here.

It is also possible to calculate the *g* and *D* tensors using DFT. In the case of the low-spin molecules, the *g* values are expected to be highly anisotropic and different from 2.00, and the values predicted by DFT (*g*_{iso} of 2.102 and 2.114 for low-spin [(cyclamacetate)FeF]⁺ and (trimethylcyclamacetate)FeF]⁺, respectively) are in agreement with this, although the calculated spread of *g* values for the former (2.2, 2.1, and 2.0) is somewhat smaller than that observed in the EPR spectrum of **1** (vide supra). On the other hand, the *g* values calculated for the high-spin species are very close to 2.00, as expected from a species in which each d orbital is singly occupied, and this agrees well with the EPR spectrum of **3**. For the high-spin molecule **3**, it is also useful to compare the calculated and observed *D* tensors. The value of *D* obtained from EPR is 0.4 cm⁻¹, which is an approximation based on the relative intensities of two bands in the spectrum. The rhombicity *E/D* (0.13) is much more well-defined because it makes the most important contribution to the general shape of the EPR spectrum. The calculated values *D* = 0.898 cm⁻¹ and *E/D* = 0.037 are reasonably close to the experimental values considering that the theory for the calculation of zero-field splittings using DFT is not yet a refined art. The sign and order of magnitude of *D* are in agreement with experiment, and the tensor is calculated to be closer to axial than to rhombic, which is also in agreement with experiment.

Previous studies have shown that Mössbauer parameters can also be extracted with surprisingly high accuracy from DFT.^{23,24} For both cations, [(cyclamacetate)FeF]⁺ and [(tri-

(22) Grapperhaus, C. A.; Bill, E.; Weyhermüller, T.; Neese, F.; Wieghardt, K. *Inorg. Chem.* **2001**, *40*, 4191.

(23) Neese, F. *Inorg. Chim. Acta* **2002**, *337*, 181.

(24) Sinnecker, S.; Slep, L. D.; Bill, E.; Neese, F. *Inorg. Chem.* **2005**, *44*, 2245.

methylcyclamacetate)FeF]⁺, DFT predicts the expected changes in isomer shift and quadrupole splitting anticipated for low-spin versus high-spin compounds. The isomer shifts for the high-spin species are calculated to be ~ 0.07 – 0.1 mm s⁻¹ higher than the low-spin species, and the high-spin species are calculated to have small quadrupole splittings of 1.0–1.2 mm s⁻¹. The experimental isomer shift and quadrupole splitting for **1** ($\delta = 0.25$ mm s⁻¹; $|\Delta E_Q| = 2.67$ mm s⁻¹) agree very well with the calculated values for the low-spin [(cyclamacetate)FeF]⁺ cation ($\delta = 0.29$ mm s⁻¹; $|\Delta E_Q| = 2.33$ mm s⁻¹), and the values for **3** ($\delta = 0.39$ mm s⁻¹; $|\Delta E_Q| = 0.95$ mm s⁻¹) agree well with the calculated values for the high-spin [(trimethylcyclamacetate)FeF]⁺ cation ($\delta = 0.43$ mm s⁻¹; $|\Delta E_Q| = 1.22$ mm s⁻¹). The calculations yield the total electric-field-gradient (EFG) tensor from which the quadrupole-splitting parameters are derived and thus also provide the sign of ΔE_Q and the asymmetry parameter η (see Tables 3 and 4). The calculated quadrupole splittings are negative, which suggests that the values for **1** and **3** are also negative. Indeed, the measurement of **3** in applied magnetic field (described above) has shown this to be true. Also, the calculated value of η for **3** (0.29) is fairly close to the value derived from experiment (0.4), showing that the shape of the EFG tensor calculated from DFT is fairly accurate. It should be mentioned that the negative quadrupole splitting observed in **3** is unexpected and counterintuitive and is opposite to what is seen in structurally similar high-spin ferric complexes of porphyrin ligands, which show almost exclusively positive quadrupole splittings.²⁵ As opposed to the ligand **II**, which is a pure σ -donor ligand, porphyrin ligands can form π bonds to the iron, through which the valence electron density from the cylindrically symmetric pair of d_{xz} and d_{yz} orbitals is removed, resulting in a greater valence charge distribution in the xy plane and a more positive contribution to the main component of the EFG (i.e., a more positive quadrupole splitting). In addition to this effect, we suggest that covalency of the Fe–F bond affects the nature of the EFG in **3**. Interestingly, the DFT calculations have reproduced the correct sign of ΔE_Q for **3**, even though its origin is not completely understood. Hyperfine coupling tensor components for **3** were also calculated from DFT, which agree very well with the experimentally determined values both qualitatively (the tensors are roughly isotropic) and quantitatively ($A_{\text{calc}} = -31.3, -31.9,$ and -32.0 MHz; $A_{\text{exp}} = -29.4, -29.4,$ and -29.0 MHz).

Why Do **1 and **3** Have Different Spin States?** Now that it has been established that the addition of *N*-methyl groups to **1** so as to produce **3** yields a change in the ground spin state from low spin to high spin, it is interesting to determine the reason for this effect. As mentioned above, Meyerstein cites four main effects of *N*-alkylation of macrocyclic ligands, two of which are solvation effects, one a steric effect, and the last an electronic effect.¹¹ Below we address each of these effects specifically.

Although it was found that solvation is the major effect influencing the solution properties of Cr and Ni complexes

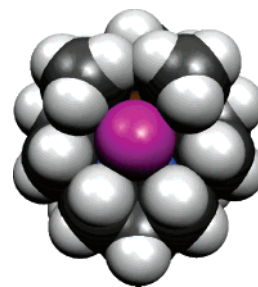


Figure 8. Space-filling view of the cation in **3** viewed from the top along the Fe–F bond. The F atom is shown in purple, Fe is brown, N is blue, C is black, and H is gray.

with cyclam or tetramethylcyclam,²¹ it is unlikely that solvation could play as drastic an effect for **1** and **3** because the observed spin states of **1** and **3** persist in the solid state.²⁶ To test the importance of solvation on **1** and **3**, we performed single-point energy calculations (B3LYP) of the cations [(cyclamacetate)FeF]⁺ and [(trimethylcyclamacetate)FeF]⁺ in both possible spin states with and without a solvation model (the COSMO model was used as described in the Experimental Section). Interestingly, as seen in Tables 3 and 4, the B3LYP calculation predicts the correct spin state for each cation *regardless of whether solvation is included*. Inclusion of COSMO alters the relative energies of the [(cyclamacetate)FeF]⁺ cation by only ~ 2 kJ mol⁻¹, whereas the energy difference between the low- and high-spin states (ΔE_S of 28 kJ mol⁻¹) is calculated to be an order of magnitude higher. As one would expect, solvation effects on [(trimethylcyclamacetate)FeF]⁺ are calculated to be less (~ 0.1 kJ mol⁻¹), and ΔE_S is about 11 kJ mol⁻¹. Thus, while solvation energies are of importance (and have been calculated to be the dominating effect in Cr and Ni cyclam complexes^{21,27}), they do not single-handedly account for the different spin states observed for **1** and **3**.

While it is difficult to quantitatively deconvolute the other factors that make up ΔE_S , it is possible to make some comments about the steric and electronic factors mentioned by Meyerstein.¹¹ Compound **3** is a sterically crowded molecule, although it may not necessarily seem so at first glance because of the deceptively simple depiction given in Figure 3. A more telling view of the cation in **3** is the space-filling view shown in Figure 8, which includes all of the hydrogen atoms. In this view, close contacts between nonbonded hydrogen atoms (2.23 Å) and between hydrogen atoms and the fluoro ligand (2.55 and 2.52 Å) become apparent.²⁸ Besides these close contacts, it should be mentioned that the calculated Fe–N bond distances of 2.090 Å in the hypothetical low-spin [(trimethylcyclamacetate)FeF]⁺ cation are not as short as the calculated Fe–N bond

(26) It should be mentioned that the solid-state structure of **1** does contain M–N–H \cdots S hydrogen bonds similar to those described by Meyerstein, but before the physical measurements were made (i.e., susceptibility or Mössbauer measurements), the sample was crushed and the interstitial solvent was removed in vacuo. Proof of this is seen in the elemental analysis of **1**, in which no solvent of methanol is found.

(27) The increased importance of solvation in the Cr and Ni complexes may be due to the fact that these form tricationic and dicationic cyclam complexes, respectively. Because the [(trimethylcyclamacetate)FeF]⁺ species are monoanions, the solvation energy is expected to be significantly lower.

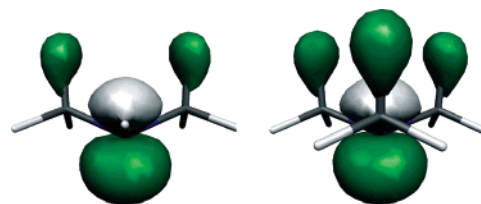
(25) Debrunner, P. G. In *Iron Porphyrins Part III*; Lever, A. B. P., Gray, H. B., Eds.; VCH: Weinheim, Germany, 1989; Vol. III, p 137.

Table 5. Electronic Properties of Me₂NH and Me₃N

	Me ₂ NH	Me ₃ N
Mulliken atomic charge on N	-0.3797	-0.3094
Mulliken reduced orbital charges:		
N s orbitals	3.50	3.49
N p orbitals	3.85	3.79
Löwdin atomic charge on N	-0.2906	-0.1738
Löwdin reduced orbital charges:		
N s orbitals	3.20	3.14
N p orbitals	4.04	3.97
natural charge on N	-0.6895	-0.5484
Composition of lone pair:		
% N s character	5.2	3.9
% N p character	68.5	63.5
% H character	13.6	18.0
relative energy of the lone pair, eV	0	+0.0057

distances in the low-spin [(cyclamacetate)FeF]⁺ cation, which lends further support to the idea that the Fe–N distances in the former species are elongated as a result of steric effects in the molecule.²⁹ This can be quantified further by comparing the calculated change of the average Fe–N bond lengths in the different spin states of the molecules ($\Delta d_{\text{Fe-N}}$). For the [(cyclamacetate)FeF]⁺ cation, $\Delta d_{\text{Fe-N}}$ is 0.15 Å, which is in good agreement with the experimental difference between **1** and **3**, and for the [(trimethylcyclamacetate)FeF]⁺ cation, $\Delta d_{\text{Fe-N}}$ is 0.13 Å, which is somewhat less. The difference of 0.02 Å could be considered to be due to steric effects, though it should be cautioned that this difference is within the error between the experimental and calculated values for **1** and **3**.

To understand the electronic effect of adding *N*-methyl groups to the ligand, simple calculations (B3LYP, double- ζ) were performed on the amines Me₂NH (dimethylamine) and Me₃N (trimethylamine). It has been previously argued that an additional alkyl group increases the donor strength of the amine ligand because methyl groups are electron-donating,¹¹ and if this is true, then the lone pair of Me₃N should be significantly higher in energy (closer in energy to where metal d orbitals are expected) and should have significantly more electron density than the lone pair of Me₂NH. Calculated electronic properties of these two amines are given in Table 5. Interestingly, the calculations imply that the N atom in Me₃N has *less* electron density than the N atom in Me₂NH because the calculated atomic charges on the N atom are less in Me₃N by ~ 0.07 and ~ 0.11 from Mulliken and Löwdin analysis, respectively. Natural population analysis confirms this result, and the calculated natural charge on N in Me₃N is 0.14 less than that in Me₂NH. This is an unexpected result and is the opposite of what is anticipated if the methyl groups are electron-donating groups. In fact, analysis of the composition of the lone pair for each amine reveals that, for each methyl group attached to the nitrogen atom, a corresponding hyperconjugation effect

**Figure 9.** Contour plots of the highest occupied molecular orbitals of the amines Me₂NH (left) and Me₃N (right). Hydrogen atoms are shown in gray, carbon atoms are shown in black, and the nitrogen atom is in the center obscured by the major lobes of the lone pair.

occurs such that one of the hydrogen atoms of the methyl group interacts in an antibonding fashion with the minor lobe of the lone pair, causing loss of N s and p character to the lone pair with the addition of each methyl group (see Figure 9). This causes the lone pair to be somewhat more contracted, and the antibonding hyperconjugation effect raises the energy of the lone pair in Me₃N by merely 0.006 eV, as compared to the analogous orbital in Me₂NH. Thus, while it is very well-known that the addition of a methyl group to a conjugated π system such as a phenyl ring causes an electron-donating inductive effect, the addition of a methyl group to an amine does not have the same effect, and in fact the hyperconjugation caused by alkylating amines causes an electron-*withdrawing* effect on the central nitrogen atom.³⁰ This electronic effect is likely responsible, in part, for the fact that the ligand **II** produces a weaker ligand field than the ligand **I**. At this time, however, it is difficult to determine whether this effect or the steric effect is the most important. Nevertheless, the longer Fe–N bond distances (a steric effect) and the weaker ligand field strength of the ligand (an electronic effect) in complexes of **II** both result in diminished orbital overlap between the amine lone-pair orbitals and the e_g iron orbitals, thus stabilizing the high-spin state relative to the low-spin state.

Conclusions

The addition of methyl groups to the ligand cyclamacetate (**I**) so as to form trimethylcyclamacetate (**II**) has the profound effect of changing the spin state of the corresponding ferric complexes. Analogous fluoro complexes of each ligand were synthesized, **1** and **3**, and their spectroscopic and magnetic properties show **1** to be low spin and **3** to be high spin. A theoretical analysis of the compounds using DFT was undertaken to determine the reason for their different spin states. The stabilization energy due to solvation was found to be greater for the nonmethylated compound, as anticipated, though DFT predicts the correct ground states for **1** and **3** regardless of whether solvation is included or not, which strongly suggests that the solvation energy is not the most important factor in determining the spin states of the compounds. Calculation of both molecules in the low-spin state leads to the interesting observation that a low-spin methylated complex would not have Fe–N bonds as short as the low-spin nonmethylated complex, which suggests that

(28) Although hydrogen atoms were placed in calculated positions in the crystal structure, geometry optimization by DFT leaves these hydrogen atoms near the positions found in the structure. Also, a close H \cdots H contact of 2.35 Å is apparent on the other side of the molecule. The van der Waals radii of H and F are 1.20 and 1.47 Å, respectively.

(29) It should also be mentioned that the difference in the calculated Fe–N distances could also be due to the systematic overestimation of the Fe–N bond distances in the methylated complex.

(30) This effect is difficult to correlate with the pK_a's of the corresponding conjugate acids H₂NMe₂⁺ and HNMe₃⁺ because solvation effects tend to dominate pK_a values measured in solution.

the Fe–N bonds are elongated in **3** because of steric reasons, which causes the high-spin state to be favored. Also, contrary to the previous claim that methyl groups add electron density to the lone pair of an amine ligand, it was found through DFT calculations that the addition of a methyl group to Me₂-NH to produce Me₃N has an electron-withdrawing effect from the nitrogen lone pair due to hyperconjugation interactions. These results support the conclusion that the difference in spin states between **1** and **3** is a combination of solvation, steric, and electronic effects and that the most important effects are likely steric and electronic.

Experimental Section

The ligand 1,4,8,11-tetraazacyclotetradecane-1-acetic acid tetrahydrochloride was synthesized according to published methods,¹² and [(cyclamacetate)FeCl]PF₆ was prepared according to the previous procedure.⁶ [NEt₄][FeCl₄] was prepared similarly to the tetrabutylammonium salt.³¹

4,8,11-Trimethyl-1,4,8,11-tetraazacyclotetradecane-1-acetic Acid Tetrahydrochloride (Trimethylcyclamacetic Acid Tetrahydrochloride). A stirred solution of 1,4,8,11-tetraazacyclotetradecane-1-acetic acid tetrahydrochloride (4.23 g, 10.5 mmol) in 25 mL of 90% formic acid and 10 mL of 35% formaldehyde was heated to 100 °C for 24 h. The resulting light-brown solution was cooled to room temperature, and the solvents were removed in vacuo. To the resulting brown residue was added 25 mL of 37% hydrochloric acid. The product was precipitated by the addition of absolute ethanol, collected by filtration, and washed with ethanol and diethyl ether. Yield: 3.35 g, 72%. IR (KBr, cm⁻¹): 3417 vs, br, 2961 s, 2633 vs, 2483 s, 1743 s (C=O), 1628 m, 1489 s, 1425 s, 1380 m, 1347 w, 1197 m, 1148 w, 1056 w, 998 w, 904 w, 778 w, 745 w, 669 w, 576 m, 546 m. ¹H NMR (D₂O, 400 MHz, d, ppm; peak assignments were made with the aid of a COSY spectrum): 3.673 s (4H, CH₂CH₂), 3.542 s (1H, CH₂COOH), 3.532 s (1H, CH₂-COOH), 3.434–3.354 m (8H, CH₂CH₂CH₂, CH₂CH₂CH₂, CH₂-CH₂), 3.112–3.101 m, br (2H, CH₂CH₂), 2.939–2.875 m (11H, 3 × CH₃, CH₂CH₂CH₂), 2.244 q (*J* = 7.45 Hz, 2H, CH₂CH₂CH₂), 1.940 q (*J* = 7.2 Hz, 2H, CH₂CH₂CH₂). ESIMS (*m/z*, amu): 300 (M – 4HCl)⁺. Anal. Calcd for C₁₅H₄₂N₄O₇Cl₄ (M·3H₂O): C, 36.01; H, 8.46; N, 11.20. Found: C, 35.60; H, 8.47; N, 11.10.

[(Cyclamacetate)FeF]PF₆ (1). To a solution of 246 mg (0.41 mmol) of [(cyclamacetate)FeCl]PF₆ in 50 mL of methanol was added 110 mg (0.43 mmol) of AgPF₆. The mixture was heated to reflux for 3 h, during which time a very fine colorless precipitate was observed. The solution was filtered through a bed of Celite and set in a crystallization dish with 20 mL of water. After 48 h, pink hexagonal crystals of **1**·MeOH were observed along with a pale-orange powder, which is the complex. Yield: 175 mg, 84%. IR (KBr, cm⁻¹): 1661 s (C=O), 840 vs (PF₆), 558 s (PF₆). ESIMS (*m/z*, amu): 809 [2M⁺ + PF₆⁻], 332 [M – PF₆]⁺, 312 [M⁺ – HF]. Anal. Calcd for C₁₂H₂₅N₄O₂FePF₇: C, 30.21; H, 5.28; N, 11.74. Found: C, 29.96; H, 5.54; N, 11.41.

(Trimethylcyclamacetate)Fe–O–FeCl₃ (2). To a suspension of trimethylcyclamacetic acid tetrahydrochloride (0.4 g, 0.897 mmol) in 30 mL of acetonitrile was added 500 μL (1.79 mmol) of triethylamine. After stirring for 1 min, a clear solution resulted. To this solution was added a solution of [NEt₄][FeCl₄] (600 mg, 1.79 mmol) in 15 mL of acetonitrile, resulting in an immediate color change to dark orange. The mixture was heated at 90 °C for

2 h, and then a second quantity of 200 μL of triethylamine was added. The dark-red mixture was heated again to 90 °C for 2 h and then allowed to cool to room temperature. The solvent was removed by rotary evaporation, and the residue was washed with diethyl ether (2 × 20 mL), cold ethanol (3 × 20 mL), and again with diethyl ether (10 mL). The resulting dark-red solid was extracted with dichloromethane, filtered, and layered with *n*-hexane. Large block-shaped crystals of (trimethylcyclamacetate)Fe–O–FeCl₃ grew over a period of days. These were collected and washed with *n*-hexane. Yield: 244 mg, 51%. IR (KBr, cm⁻¹): 3443 m, br, 3024 w, 2995 w, 2866 w, br, 1671 vs (C=O), 1470 m, 1392 w, 1349 m, 1321 m, 1306 m, 1253 w, 1229 w, 1199 w, 1170 w, 1151 w, 1123 m, 1107 w, 1093 w, 1071 w, 1058 w, 1037 w, 1024 w, 1001 w, 986 w, 970 m, 962 m, 939 w, 923 w, 912 w, 844 s, 832 s (Fe–O–Fe), 788 w, 758 w, 744 w, 713 w, 549 w, 508 w, 478 w, 420 w. ESIMS (*m/z*, amu): 569 (M + Cl)⁺. Anal. Calcd for C₁₅H₃₁O₃N₄Fe₂Cl₃: C, 33.77; H, 5.86; N, 10.50. Found: C, 34.20; H, 5.46; N, 10.12.

[(Trimethylcyclamacetate)FeF]PF₆ (3). A solution of (trimethylcyclamacetate)Fe–O–FeCl₃ (0.100 g, 0.188 mmol) in 25 mL of water was treated with KPF₆ (0.208 mg, 1.13 mmol), causing the precipitation of some light-orange solids (rust). Filtration yielded a bright-yellow solution, from which the fluoro complex crystallized as small yellow plates upon slow evaporation of the solvent in air. Yield: 33 mg, 34%. IR (KBr, cm⁻¹): 3455 w, br, 2969, w, 1682 s (C=O), 1470 m, 1338 w, 1298 s, 1262 w, 1154 w, 1107 w, 1092 w, 1059 w, 1023 w, 969 w, 918 w, 841 vs (PF₆), 822 s, 746 w, 712 w, 558 s (PF₆), 543 m. ESIMS (*m/z*, amu): 374 (M – PF₆)⁺. Anal. Calcd for C₁₅H₃₁O₂N₄FePF₇: C, 34.70; H, 6.02; N, 10.79. Found: C, 34.80; H, 6.10; N, 10.58.

Physical Measurements. IR spectra were taken in the range of 400–4000 cm⁻¹ on a Perkin-Elmer 2000 FT-IR/FT-NIR spectrometer on samples pressed into KBr disks. ¹H, ¹³C, and COSY NMR spectra were recorded on a Bruker 400-MHz AMX series spectrometer. ESIMS spectra were obtained on a Finnigan MAT 95 spectrometer. Elemental analyses were done by the H. Kolbe Mikroanalytisches Laboratorium in Mülheim an der Ruhr, Germany. Temperature-dependent magnetic susceptibilities were measured on a Quantum Design SQUID magnetometer in the temperature range of 2–350 K at an applied external field of 0.1 T. Data points were corrected for intrinsic diamagnetism of the sample and the sample holder and also for temperature-independent paramagnetism (TIP). X-band EPR spectra were recorded at 10 K on a Bruker ESP 300E spectrometer equipped with a helium-flow cryostat (Oxford Instruments ESR 910), which was used for regulation of the temperature and for the variable-temperature measurements. Mössbauer spectra were recorded on an alternating constant-acceleration spectrometer with a minimum line width of 0.24 mm s⁻¹. The sample temperature was maintained by an Oxford Instruments Variox cryostat or an Oxford Instruments Mössbauer-Spectromag 2000 cryostat. The latter was used for measurement in applied magnetic fields with the field oriented perpendicular to the γ source. Isomer shifts (δ) are referenced against iron metal at 300 K.

X-ray Crystallography. Crystal data are listed in Table 6. A crystal of **1** was mounted at the tip of a quartz fiber and transferred to the goniometer of a Bruker SMART CCD detector system, where it was cooled by a cryogenic nitrogen stream to 100 K for data collection. Graphite-monochromated Mo K α radiation (λ = 0.710 73 Å) was used for the experiments. The data were collected using SMART software,³² processed using SAINTPLUS software,³³ and

(31) Grapperhaus, C. A.; Li, M.; Patra, A. K.; Poturovic, S.; Kozlowski, P. M.; Zgierski, M. Z.; Mashuta, M. S. *Inorg. Chem.* **2003**, *42*, 4382.

(32) SMART, version 5.618; Bruker Analytical X-ray Systems, Inc.: Madison, WI, 1998.

Table 6. Crystal Data

	1•MeOH	2	3
formula	C ₁₃ H ₂₉ F ₇ FeN ₄ O ₃ P	C ₁₅ H ₃₁ Cl ₃ Fe ₂ N ₄ O ₃	C ₁₅ H ₃₁ F ₇ FeN ₄ O ₂ P
fw	509.22	533.49	519.26
cryst syst	monoclinic	orthorhombic	orthorhombic
space group	<i>P</i> 2 ₁ / <i>c</i>	<i>P</i> 2 ₁ 2 ₁ 2 ₁	<i>Pnma</i>
<i>a</i> , Å	11.2520(9)	8.9070(4)	12.4880(4)
<i>b</i> , Å	20.464(2)	13.6850(6)	11.0202(3)
<i>c</i> , Å	8.9153(9)	18.6935(8)	15.0237(5)
β , deg	98.16(1)	90	90
<i>V</i> , Å ³	2032.1(3)	2278.6(2)	2067.6(1)
<i>Z</i>	4	4	4
<i>d</i> (calcd), g cm ⁻³	1.664	1.555	1.668
Flack parameter		0.01(2)	
R1, ^a wR2 ^b (<i>I</i> > 2σ(<i>I</i>))	0.0477, 0.0979	0.0412, 0.0694	0.0453, 0.0793
R1, ^a wR2 ^b (all data)	0.0867, 0.1108	0.0521, 0.0722	0.0669, 0.0864

$${}^a R1 = \sum ||F_o| - |F_c|| / \sum |F_o|. \quad {}^b wR2 = [\sum [w(F_o^2 - F_c^2)^2] / \sum [w(F_o^2)^2]]^{1/2}, \quad w = 1/\sigma^2(F_o^2) + (aP)^2 + bP, \quad \text{where } P = [\max(0 \text{ or } F_o^2) + 2(F_c^2)]/3.$$

corrected for absorption using the program *SADABS*.³⁴ Crystals of **2** and **3** were each, in turn, mounted on the goniometer of a Nonius Kappa CCD detector system and were cooled to 100 K for data collection. The data for **2** and **3** were not corrected for absorption. The structures were all solved via the direct methods routine in the *SHELXTL97* program package³⁵ and refined using difference Fourier techniques. Hydrogen atoms were placed in calculated positions in the structure and refined using a riding model. The trimethylcyclamacetate ligand was found to be disordered in two orientations in **2**. Thermal ellipsoids for corresponding atoms in each orientation were constrained to have the same displacement parameters, and interatomic distances for both orientations were restrained to have the same value within an estimated standard deviation of 0.01 Å.

Computations. The cations [(cyclamacetate)FeF]⁺ and [(trimethylcyclamacetate)FeF]⁺ were used for DFT calculations assuming either an *S* = 1/2 or 5/2 ground state for each. The calculations were performed using the *ORCA* program package.³⁶ The initial geometries for each cation were taken from their respective crystal structures, and geometry optimization was carried out on these structures at the BP86 level of theory using the default polarized double- and triple- ζ basis sets³⁷ in the *ORCA* package. The triple- ζ -optimized geometries were then used for calculation of energies and properties. Vibrational frequencies were calculated at the BP86 level using a numerical differentiation of analytical

gradients with an increment of 0.005 bohr. No negative frequencies were observed, indicating that the structures correspond to potential energy minima. Total energies were calculated at the optimized geometries with the B3LYP functional (triple- ζ). Zero-point vibrational energies and thermal corrections were taken from the preceding frequency calculations. Solvent effects were estimated at the level of a dielectric continuum approach using the COSMO model²⁰ with $\epsilon = 36.6$ modeling acetonitrile. Natural atomic orbital and natural bond orbital analyses were performed to determine natural charges using the *NBO* program.³⁸ Mössbauer parameters were calculated at the B3LYP level [using a triple- ζ basis set and the CP(PPP) basis set²³ for iron] as described previously.²³ The *g* values and *D* tensors were calculated according to previously developed procedures.³⁹ Orbitals were visualized with the *MOLEKEL* program.⁴⁰

Acknowledgment. We thank the Fonds der Chemischen Industrie for financial support. J.F.B. thanks the Alexander von Humboldt Foundation for a postdoctoral fellowship.

Supporting Information Available: Crystallographic data for **1–3** in CIF format. Variable-temperature Mössbauer spectra of **1** and a table of the parameters derived from them. This material is available free of charge via the Internet at <http://pubs.acs.org>.

IC051823Y

(33) *SAINTPPLUS*, version 6.45A; Bruker Analytical X-ray Systems, Inc.: Madison, WI, 1998.

(34) Blessing, R. H. *Acta Crystallogr., Sect. A* **1995**, *51*, 33.

(35) Sheldrick, G. M. *SHELXTL97*; University of Göttingen: Göttingen, Germany, 1997.

(36) Neese, F. *ORCA—an ab initio, DFT, and Semiempirical Electronic Structure Package*, version 2.2; Max-Planck-Institut für Strahlenchemie: Mülheim, Germany, 2003.

(37) Schafer, A.; Horn, H.; Ahlrichs, R. *J. Chem. Phys.* **1992**, *97*, 2571.

(38) Glendening, E. D.; Badenhoop, J. K.; Reed, A. E.; Carpenter, J. E.; Bohmann, J. A.; Morales, C. M.; Weinhold, F. *NBO*, version 5.0; Madison, WI, 2001.

(39) (a) Neese, F. *J. Chem. Phys.* **2001**, *115*, 11080. (b) Schöneboom, J. C.; Neese, F.; Thiel, W. *J. Am. Chem. Soc.* **2005**, *127*, 5840. (c) Neese, F.; Solomon, E. I. *Inorg. Chem.* **1998**, *37*, 6568.

(40) Flükiger, P.; Lüthi, H. P.; Portmann, S.; Weber, J. *MOLEKEL*, version 4.0; Swiss Center for Scientific Computing: Manno, Switzerland, 2000.